Received: 16 January 2018 | Revised: 9 March 2018 | Accepted: 12 March 2018

DOI: 10.1002/aoc.4382

FULL PAPER

WILEY Applied Organometallic Chemistry

Synthesis, characterization and theoretical and fluorescence emission microscopy studies of new Pd/Pt–cyclopropa[60] fullerene complexes: Application of Taguchi method for optimization of parameters in Suzuki–Miyaura reaction

Seyyed Javad Sabounchei[1] | Khadijeh Badpa[1] | Ali Hashemi[1] | Sadegh Salehzadeh[1] | Farahnaz Maleki[1] | Leila Hosseinzadeh[2]

[1] Faculty of Chemistry, Bu-Ali Sina University, Hamedan 65174, Iran

[2] Pharmaceutical Sciences Research Center, Kermanshah University of Medical Sciences, Kermanshah, Iran

Correspondence
Seyyed Javad Sabounchei, Faculty of Chemistry, Bu-Ali Sina University, Hamedan 65174, Iran.
Email: jsabounchei@yahoo.co.uk

Funding information
Bu-Ali Sina University

The reactions of unsymmetric phosphorus ylides of the type $[Ph_2P(CH_2)_nPPh_2{=}C(H)C(O)C_6H_4\text{-}p\text{-}CN]$ (n = 1 (Y^1); n = 2 (Y^2)) with C_{60} and $M(dba)_2$ (M = Pd or Pt; dba = dibenzylideneacetone) are reported. Based on the various coordination modes of these ylides in complexation, the following new Pd/Pt–cyclopropa[60]fullerene complexes were obtained: P,C-coordinated $[(\eta^2\text{-}C_{60})Pd(\kappa^2\text{-}Y^1)]$ (**1**) and $[(\eta^2\text{-}C_{60})Pt(\kappa^2\text{-}Y^1)]$ (**2**) complexes and P-coordinated $[(\eta^2\text{-}C_{60})Pd(Y^2)_2]$ (**3**) and $[(\eta^2\text{-}C_{60})Pt(Y^2)_2]$ (**4**) complexes. These compounds were characterized using Fourier transform infrared, UV–visible and NMR (^1H, ^{13}C and ^{31}P) spectroscopies and scanning electron microscopy. Furthermore, cytotoxicity studies showed that nanoparticles of these complexes can be used as non-toxic labels for cellular imaging application. Also energy decomposition analysis results revealed that the percentage contribution of ΔE_{elec} in total interaction energy is considerably larger than that of ΔE_{orb}. Thus, in all complexes the $(\eta^2\text{-}C_{60})M\text{—}(Y^1)$ bond is considerably more electrostatic in nature than the $(\eta^2\text{-}C_{60})\text{—}M(Y^1)$ bond. Finally, by application of the Taguchi method for optimization of parameters in Suzuki–Miyaura reaction, the catalytic activity of Pd complexes **1** and **3** was investigated in the cross-coupling reaction of various aryl chlorides with phenylboronic acid. According to analysis of variance results, solvent has the highest F value and it has high contribution percentage (36.75%) to the yield of Suzuki–Miyaura reaction.

KEYWORDS
Pd/Pt–cyclopropa[60]fullerene complexes, Suzuki–Miyaura reaction, synthesis, Taguchi method, theoretical studies

1 | INTRODUCTION

After the discovery of C_{60} in 1985 by Kroto *et al.*,[1] fullerenes have attracted a tremendous amount of research interest due to their interesting physicochemical, optical, mechanical and electrical properties.[2–6] Moreover, metalla-cyclopropa[60]fullerenes, in which the fullerene cage is attached to a metal centre to form corresponding organometallic π-complexes,[7–15] have become a current focus of fullerene research into important roles in

biological and materials science.[16,17] Among such complexes, Pd/Pt–cyclopropa[60]fullerene complexes that contain phosphorus ligands have received less attention. Thus, the search for improved methods for the synthesis of these transition metal–fullerene complexes is of considerable importance. Experimental and theoretical studies of the reactivity and coordination chemistry of carbonyl-stabilized phosphorus ylides are an important research field of our group.[18–23] Because of various coordination modes of α-keto-stabilized phosphorus ylides in metal complexes (P-, C- and P,C-coordination modes), these compounds are attractive candidates for further development in Pd/Pt–cyclopropa[60]fullerene complexes.[24,25]

During the past few years, significant progress has been made in the use of Pt–cyclopropa[60]fullerene complexes in some biological applications.[26–30] Based on cytomorphological studies, Pt–cyclopropa[60]fullerene complexes can be used as effective platforms for drug delivery to molecular targets in tumour cells.[31,32] However, *in vitro* and *in vivo* detection of these nanomaterials is particularly difficult using standard fluorescence microscopy, because their solubility is low and fluorescence is barely detectable.[33] Use of specific Pt–cyclopropa[60]fullerene complexes for targeted delivery of drugs to tumour cells is one of the most appropriate ways for reducing severe toxicity of conventional anticancer drugs towards normal tissues.[33]

There are some reports in which Pd–cyclopropa[60]fullerene complexes have been used as efficient catalysts for a variety of reactions.[27] For example, Sulman and co-workers investigated experimentally and theoretically the catalytic activity of η^2-$C_{60}Pd(PPh_3)_2$ complex in selective hydrogenation of acetylenic alcohols.[34] Also, Veisi *et al*. reported the synthesis of biguanide (metformine)-functionalized fullerene (C_{60}-Met/Pd^{2+}) complexes and their application in the Suzuki–Miyaura coupling reaction of various aryl halides and phenylboronic acid. The Suzuki–Miyaura reaction, one of the most popular and powerful methods for the joining of aryl–aryl moieties, is typically catalysed by palladium complexes containing bulky and electron-rich phosphine ligands. This reaction appears to be affected by various parameters, including solvent, base and catalyst loading, and a systematic study of the optimization of these factors with the Taguchi method makes it possible to investigate the contribution percentage of desired parameters to the yield of the reaction. The Taguchi method, a robust design approach, uses many ideas from statistical experimental design for evaluating and implementing improvements in processes[35] and it can help in appropriate selection of conditions for the Suzuki–Miyaura reaction.

Based on the above considerations, we aimed to use Pd–cyclopropa[60]fullerene complexes bearing unsymmetric phosphorus ylides in Taguchi-optimized Suzuki–Miyaura reactions. Herein, we report the synthesis, characterization and theoretical and catalytic studies of new Pd/Pt–[60]fullerene complexes of mono- and bidentate phosphorus ylides (Figure 1).

2 | EXPERIMENTAL

2.1 | Materials and Methods

All synthetic reactions were carried out under an atmosphere of dry nitrogen using standard Schlenk techniques. C_{60} (+99.5%) and $M(dba)_2$ (M = Pd or Pt; dba = dibenzylideneacetone) were obtained from commercial sources and used without further purification. Phosphorus ylides Y^1 and Y^2 were synthesized and characterized as previously reported.[36] Toluene and *n*-hexane were used as reagent grade and dried over Na/benzophenone. NMR (^1H, ^{13}C and ^{31}P) spectra were recorded using 250 MHz Bruker and 90 MHz Jeol spectrometers with $CDCl_3$ as solvent at 25 °C. Infrared (IR) spectra were recorded with a PerkinElmer FT-IR spectrophotometer in the range 400–4000 cm^{-1} using KBr pellets. UV–visible spectra were recorded between 200 and 800 nm using a Perkin voyager DE-PRO spectrometer. Scanning electron microscopy (SEM) was conducted using a VEGA TESCAN instrument.

2.2 | Synthesis of Pd/Pt–[60]Fullerene Complexes

In a general procedure, a toluene solution of $M(dba)_2$ (M = Pd or Pt; 0.05 mmol, 5 ml) was added to a toluene solution of C_{60} (0.036 g, 0.05 mmol, 15 ml) and the resulting black suspension was stirred in a 50 ml Schlenk tube at ambient temperature. After 15 min, a solution of ylide was injected into the system via a syringe pump (0.05 mmol, 5 ml). The solution was further stirred for 2 h at room temperature. The solid product can be precipitated from the deep-green solution with a non-polar solvent such as *n*-hexane. The obtained solid was then washed with diethyl ether to afford the desired pure product.

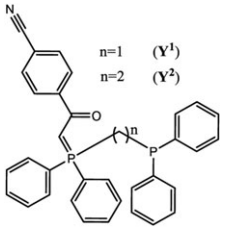

FIGURE 1 Phosphorus ylides that were applied in this study as ligands

2.2.1 | Data for $[(\eta^2\text{-}C_{60})Pd(\kappa^2\text{-}Y^1)]$ (1)

Black solid; yield 0.051 g (91%); m.p. > 300 °C (decomposed). Selected IR data (KBr, cm^{-1}): 1650 (C=O), 524 (C_{60}). UV–visible in toluene (λ_{max}, nm): 300, 314, 360. ^1H NMR (250.13 MHz, $CDCl_3$, δ_H, ppm): 4.26 (m, 2H, CH_2); 5.53 (d, 1H, PCH); 6.71–7.93 (m, 24H, Ph). ^{13}C NMR ($CDCl_3$, δ_C, ppm): 22.66 (s, CH_2); 31.90 (d, PCH,); 119 (s, CN); 125.27–143.08 (Ph and C_{60}); 187.1 (s, CO). ^{31}P NMR ($CDCl_3$, δ_P, ppm): 13.18 (d, PCH, $^2J_{P-P}$ = 79.68 Hz); 31.26 (d, PPh_2, $^1J_{P-P}$ = 79.68 Hz).

2.2.2 | Data for $[(\eta^2\text{-}C_{60})Pt(\kappa^2\text{-}Y^1)]$ (2)

Black solid; yield 0.051 g (73%); m.p. > 300 °C (decomposed). Selected IR data (KBr, cm^{-1}): 1651 (C=O); 526 (C_{60}). UV–visible in toluene (λ_{max}, nm): 302, 322. ^1H NMR ($CDCl_3$, δ_H, ppm): 4.80 (m, 2H); 5.85 (d, 1H, PCH); 6.98–8.59 (m, 24H, Ph). ^{13}C NMR ($CDCl_3$, δ_C, ppm): 38.70 (s, CH_2); 56 (d, PCH); 112.8 (s, CN); 127.2–141.2 (Ph and C_{60}); 188.53 (s, CO). ^{31}P NMR ($CDCl_3$, δ_P, ppm): 13.27(td, PCH, $^1J_{Pt-P}$ = 3920.8 Hz); 40.42 (d, PPh_2, $^2J_{Pt-P}$ = 66.6 Hz).

2.2.3 | Data for $[(\eta^2\text{-}C_{60})Pd(Y^2)_2]$ (3)

Black solid; yield 0.075 g (75%); m.p. > 300 °C (decomposed). Selected IR data (KBr, cm^{-1}): 1618 (C=O); 512 (C_{60}). UV–visible in toluene (λ_{max}, nm): 298, 334, 354. ^1H NMR ($CDCl_3$, δ_H, ppm): 2.81 (m, 4H, CH_2); 4.13 (m, 1H, CH); 7.06–7.99 (m, 24H, Ph). ^{13}C NMR ($CDCl_3$, δ_C, ppm): 21.41 (m, CH_2); 49.20 (d, CH); 119.11 (s, CN); 124.90–148.66 (Ph and C_{60}); 182.75 (s, CO). ^{31}P NMR ($CDCl_3$, δ_P, ppm): 16.73 (d, PCH); 17.69 (d, pph_2).

2.2.4 | Data for $[(\eta^2\text{-}C_{60})Pt(Y^2)_2]$ (4)

Black solid; yield 0.043 g (87%); m.p. > 300 °C (decomposed). Selected IR data (KBr, cm^{-1}): 1617 (C=O); 524 (C_{60}). UV–visible in toluene (λ_{max}, nm): 302, 334. ^1H NMR ($CDCl_3$, δ_H, ppm): 2.73 (m, 4H, CH_2); 4.12 (d, 1H, CH); 7.07–8.34 (m, 24H, Ph). ^{13}C NMR ($CDCl_3$, δ_C, ppm): 21.45 (m, CH_2); 49.04 (d, CH); 119.08 (s, CN); 124.18–147.36 (Ph and C_{60}); 182.94 (s, CO). ^{31}P NMR ($CDCl_3$, δ_P, ppm): 16.46 (td, PPh_2, $^1J_{Pt-P}$ = 3208.2 Hz): 19.21 (td, PPh_2, $^2J_{Pt-P}$ = 3872.7 Hz).

2.3 | Cytotoxicity and Cellular Uptake Assay

Human umbilical vein endothelial cells (HUVEC cell line) were obtained from Pasteur Institute of Iran (Tehran, Iran). Dulbecco's modified Eagle's medium (DMEM-F12) supplemented with foetal bovine serum (10% *v*/v) and 1% penicillin (100 U ml^{-1})–streptomycin (100 U ml^{-1}) was used for cell growth at 37 °C in a humidified incubator

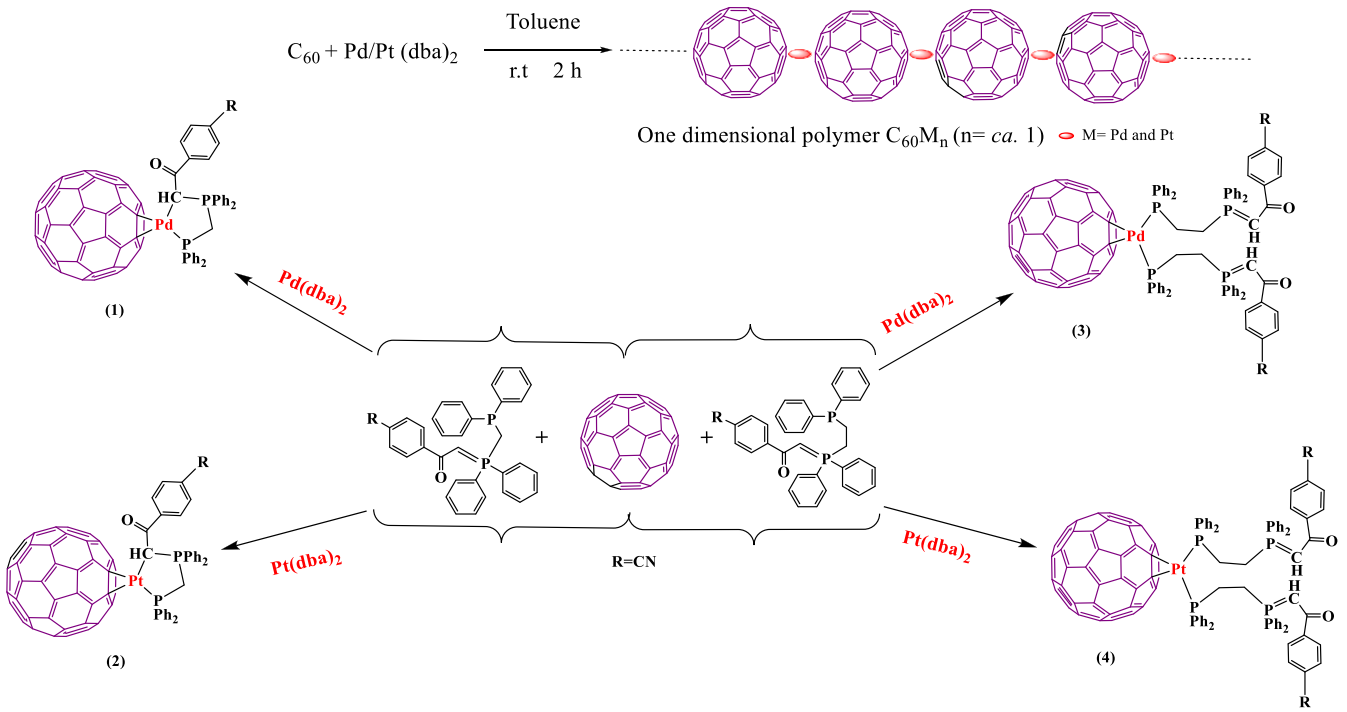

SCHEME 1 Synthesis of metallo-cyclopropa[60]fullerene complexes **1–4**

containing 5% CO_2. Cell proliferation was determined using the 3-(4,5-dimethylthiazol-2-yl)-2,5-diphenyltetrazoliumbromide (MTT) assay. The cells were plated in 96-well cell culture plates at a cell density of 15×10^4 cells per well. After 24 h the spent medium was replaced with fresh medium containing increasing concentrations (0–200 μM) of compounds **1** and **2**. A negative control of untreated cells was included. The cells were incubated for a further 24 h, after which a 0.5 mg ml^{-1} MTT solution (10 μl per well) was added and the cells incubated for an additional 4 h. Then, the medium was removed, and the purple formazan crystals were dissolved in dimethylsulfoxide (200 μl per well). Absorbance was determined using an ELISA plate reader (Biotek H1 M) with a test wavelength of 570 nm and a reference wavelength of 630 nm to obtain sample signal (OD570 − OD630). For evaluation of cellular uptake, HUVECs were plated in 6-well cell culture plates at a cell density of 7×10^5 cells per well. After leaving overnight, cells were treated with the compounds at a concentration of 200 μM and then the plates were transferred to a 37 °C incubator for 4 h. After that fluorescence images were

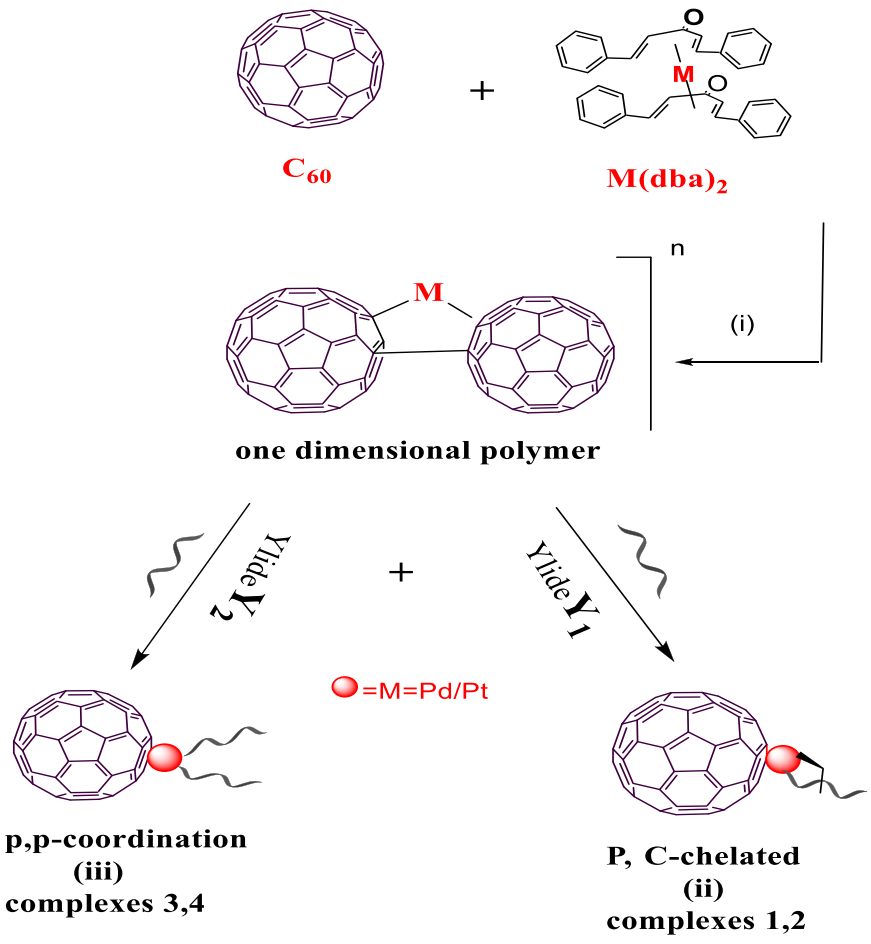

SCHEME 2 Proposed pathway for synthesis of complexes **1–4**

TABLE 1 Spectroscopic data for compounds Y^1, Y^2 and **1–4**

Compound	IR; ν(CO) (cm^{-1})	^{1}H NMR; δ(PCH) (ppm)	^{13}C NMR; δ(CO) (ppm)	^{31}P NMR; δ(PCH) and (PPh_2) (ppm)
Y^1	1572	4.33	183.18	15.35, −29.48
1	1650	5.53	187.1	13.18, 31.26
2	1651	5.85	188.53	13.27, 40.42
Y^2	1570	4.26	188.79	17.18, −12.83
3	1618	4.13	182.75	16.73, 17.69
4	1617	4.12	182.94	16.46, 19.21

obtained at ×100 magnification using a fluorescence microscope (Micros, Austria) with imaging system. Cells without any treatment were taken as a staining control.

2.4 | Suzuki–Miyaura Coupling Reaction

In a general procedure, to a round-bottom flask equipped with a magnetic stirring bar a mixture of Pd–[60]fullerene complex (0.005 mmol), phenylboronic acid (1 mmol), aryl chloride (0.75 mmol) and K_2CO_3 (1.5 mmol) in dimethylformamide (DMF; 2 ml) was added. The mixture was heated to 130 °C for 2 h in the presence of air and the progress was monitored by TLC. After completing the cross-coupling reaction, the mixture was diluted with *n*-hexane–water (50:50). The organic layer was washed with brine (15 ml) and dried over $CaCl_2$. The solvent was evaporated and the crude product purified by recrystallization from ethanol and water or purified by silica gel column chromatography (*n*-hexane–EtOAc, 80:20).

2.4.1 | Data for 4-nitrobiphenyl (5a)

M.p. 112–113 °C. ^{1}H NMR (89.6 MHz, $CDCl_3$, δ_H, ppm): 7.26–8.34 (m, 9H, phenyl). ^{13}C NMR (62.89 MHz, $CDCl_3$, δ_C, ppm): 147.68, 146.97, 128.92, 127.84, 124.10.

2.4.2 | Data for 4-phenylbenzaldehyde (5b)

M.p. 89–91 °C. ^{1}H NMR (89.6 MHz, $CDCl_3$, δ_H, ppm): 9.91 (s, 1H, CHO), 7.30–7.86 (m, 9H, phenyl). ^{13}C NMR (100.62 MHz, $CDCl_3$, δ_C, ppm): 191.91 (s, CO), 147.09, 139.60, 135.07, 130.21, 128.95, 128.41, 127.60, 127.29.

2.4.3 | Data for biphenyl (5c)

M.p. 67–69 °C. ^{1}H NMR (89.6 MHz, $CDCl_3$, δ_H, ppm): 7.01–7.51 (m, 10H, phenyl). ^{13}C NMR (100.62 MHz, $CDCl_3$, δ_C, ppm): 141.29, 128.8, 127.30, 127.22.

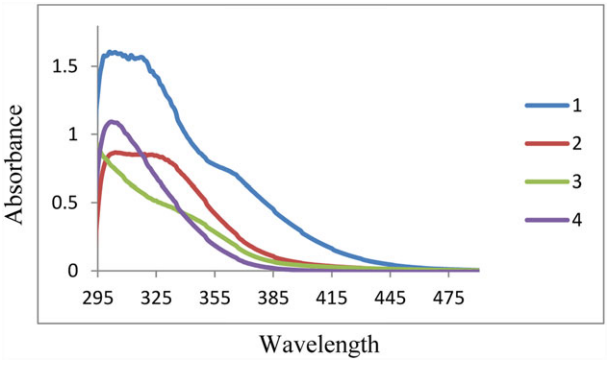

FIGURE 2 The UV–Vis spectral data of complexes **1–4**

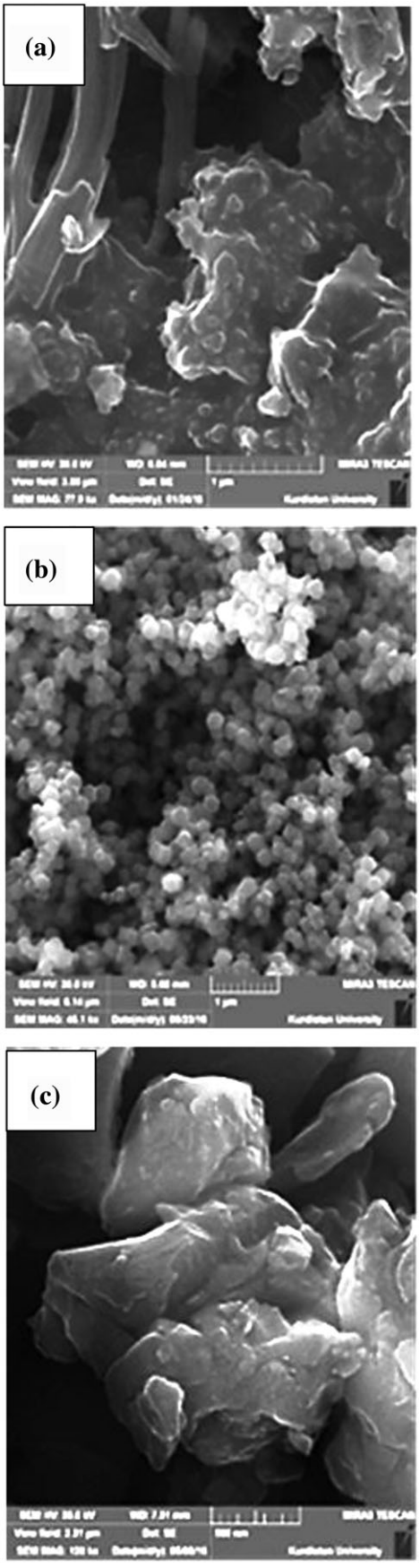

FIGURE 3 SEM images of (a) C_{60}, and (b) complex **3**(1 μm) and **(c)** complex **3** (500 nm)

2.4.4 | Data for 4-phenylcarboxylic acid (5d)

M.p. 223–226 °C. ^{1}H NMR (89.6 MHz, $CDCl_3$, δ_H, ppm): 11.03 (s, COOH, 1H), 7.31–7.88 (m, phenyl, 9H). ^{13}C NMR (100 MHz, $CDCl_3$, δ_C, ppm): 163.3 (s, C═O), 144.8 (s, phenyl), 139.8 (s, phenyl), 129.58 (s, phenyl), 129.13 (s, phenyl), 127.47 (s, phenyl), 126.9 (s, phenyl), 124.3 (s, phenyl).

2.4.5 | Data for 4-acetylbiphenyl (5e)

M.p. 117–118 °C. ^{1}H NMR (300 MHz, $CDCl_3$, δ_H, ppm): 8.02–8.05 (m, phenyl, 2H), 7.62–7.70 (m, phenyl, 4H), 7.26–7.50 (m, phenyl, 3H), 2.64 (s, CH_3, 3H). ^{13}C NMR (100 MHz, $CDCl_3$, δ_C, ppm): 197.5 (s, C═O), 145.8 (s, phenyl), 139.7 (s, phenyl), 135.6 (s, phenyl), 128.83 (s, phenyl), 128.79 (s, phenyl), 128.11 (s, phenyl), 127.15 (s, phenyl), 127.10 (s, phenyl), 26.7 (s, CH_3).

3 | RESULTS AND DISCUSSION

3.1 | Synthesis

The synthetic procedure for target compounds **1**–**4** consists of two steps. (1) Reaction of [60]fullerene with $M(dba)_2$ (M = Pd or Pt) which resulted in facile displacement of the dba ligand and formation of black–brown insoluble $(C_{60}Pd/Pt)_n$ polymer.[37,38] (2) Further reaction of phosphorus ylides with $(C_{60}Pd/Pt)_n$ polymer which led to formation of deep-green solution of Pd/Pt–[60]fullerene complexes. It is worth mentioning that reaction of phosphorus ylide Y^1 with $(C_{60}Pd/Pt)_n$ polymer gave the P,C-coordinated complexes **1** and **2**, whereas similar reaction of ylide Y^2 with $(C_{60}Pd/Pt)_n$ polymer led to formation of the P-coordinated complexes **3** and **4** (Scheme 1).

A view of the proposed pathway for the synthesis of the Pd/Pt–[60]fullerene complexes is depicted in Scheme 2. (i) Firstly, the black and insoluble polymer $(C_{60}Pd/Pt)_n$ was obtained from the reaction of C_{60} and $M(dba)_2$.[39] (ii) Terminal PPh_2 group of phosphorus ylides was coordinated to metallic centre of $(C_{60}M)_n$. In the case of phosphorus ylide Y^1, this was followed

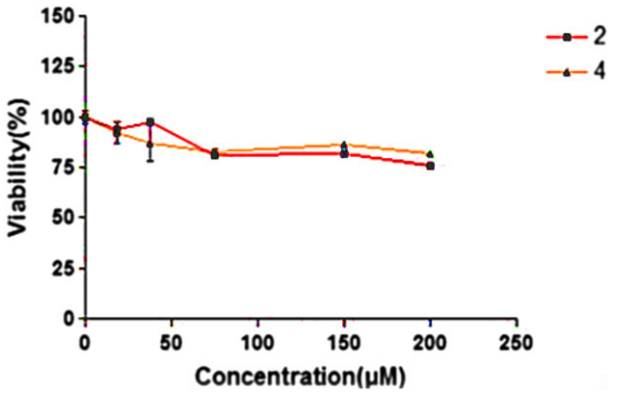

FIGURE 4 Effects of compound **2** and **4** on the Human umbilical vein endothelial cells viability. HUVEC cells were incubated with different concentrations of the compounds for 24 h. The cell proliferation inhibition was determined by MTT assay as described under materials and methods. Data are presented as mean ± S.E.M (n = 3)

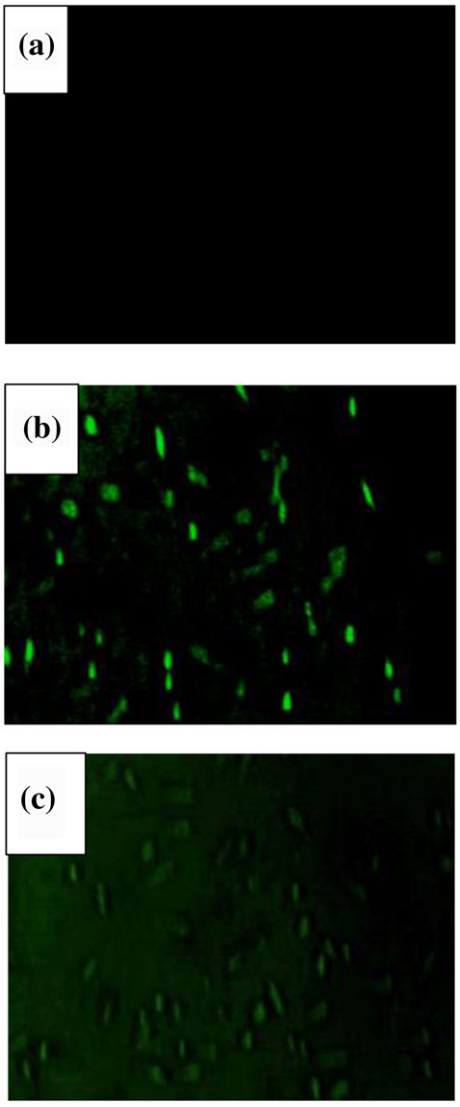

FIGURE 5 A) Effects of compound **2** and **4** on the Human umbilical vein endothelial cells viability. HUVEC cells were incubated with different concentrations of the compounds for 24 h. The cell proliferation inhibition was determined by MTT assay as described under materials and methods. Data are presented as mean ± S.E.M (n = 3). B) Fluoroescence microscope images demonstrating the intracellular nanoparticles distribution in HUVEC cell line. (a) Control cells incubated without compound. (b) Cells exposed to compound **1** and (c) compound **2** for 4 h

by chelation of the ylide through carbon and formation of P,C-coordinated complexes **1** and **2**. (iii) In the case of phosphorus ylide Y^2, formation of P,C-chelated complex is not favourable and a second ligand was added which led to formation of P-coordinated complexes **3** and **4**.

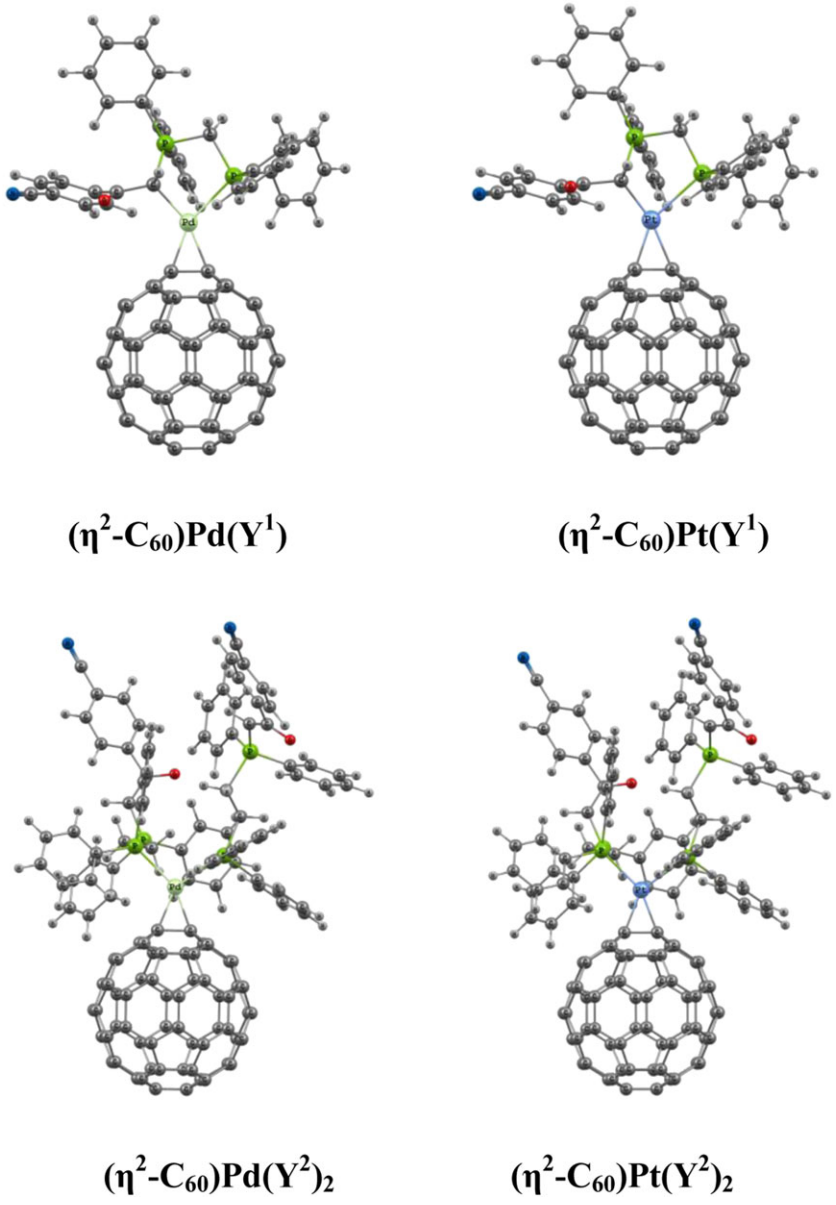

FIGURE 6 The optimized structure of $(\eta^2\text{-}C_{60})M(Y^1)$, $(\eta^2\text{-}C_{60})M(Y^2)$, $(\eta^2\text{-}C_{60})M(Y^1)_2$ and $(\eta^2\text{-}C_{60})M(Y^2)_2$ (M = Pd and Pt) complexes

TABLE 2 Results of EDA (kcal mol^{-1}) at BP86-D3/TZP//BP86/LANL2MB level

Complex	Fragments	ΔE_{int}	ΔE_{Pauli}	ΔE_{elec}	ΔE_{orb}	ΔE_{disp}
$(\eta^2\text{-}C_{60})Pd(Y^1)$	$(\eta^2\text{-}C_{60})Pd...(Y^1)$	−73.86	135.10	−128.47 (61.5%)	−62.73 (30.0%)	−17.77 (8.5%)
	$(\eta^2\text{-}C_{60})...Pd(Y^1)$	−64.26	156.70	−113.73 (51.5%)	−92.92 (42.1%)	−14.32 (6.5%)
$(\eta^2\text{-}C_{60})Pt(Y^1)$	$(\eta^2\text{-}C_{60})Pt...(Y^1)$	−104.47	204.24	−186.00 (60.3%)	−102.25 (33.1%)	−20.45 (6.6%)
	$(\eta^2\text{-}C_{60})...Pt(Y^1)$	−84.13	194.96	−138.63 (49.7%)	−123.03 (44.1%)	−17.42 (6.2%)
$(\eta^2\text{-}C_{60})Pd(Y^2)_2$	$(\eta^2\text{-}C_{60})Pd...(Y^3)_2$	−74.56	90.14	−88.06 (53.5%)	−49.74 (30.2%)	−26.91 (16.3%)
	$(\eta^2\text{-}C_{60})...Pd(Y^3)_2$	−71.16	172.83	−125.46 (51.4%)	−95.86 (39.3%)	−22.68 (9.3%)
$(\eta^2\text{-}C_{60})Pt(Y^2)_2$	$(\eta^2\text{-}C_{60})Pt...(Y^3)_2$	−101.68	127.15	−118.50 (51.8%)	−79.91 (34.9%)	−30.42 (13.3%)
	$(\eta^2\text{-}C_{60})...Pt(Y^3)_2$	−101.53	225.84	−164.61 (50.3%)	−136.45 (41.7%)	−26.31 (8.0%)

3.2 | Characterization

The products were identified with NMR (^{1}H, ^{13}C and ^{31}P) and IR spectroscopic methods and the data are summarized in Table 1. These results provide a useful comparison between the data relating to parent phosphorus ylides Y^1 and Y^2 and compounds **1**–**4**.

3.2.1 | IR spectra

By paying attention to the changes of ν(CO) region in the IR spectra of complexes **1** and **2** compared to ylide Y^1, it is confirmed that coordination of the ylide has occurred simultaneously through the ylidic carbon and PPh_2 groups.[40] However, the IR spectra of complexes **3** and **4** did not show any significant frequency shift compared to parent ylide Y^2 which suggests that the coordination of the ylide occurs only through the PPh_2 groups (see supporting information). Also, it is worth mentioning that the IR spectra of all complexes displayed the characteristic absorption bands of C_{60} core at around 526, 579, 1184 and 1435 cm^{-1}.

3.2.2 | NMR spectra

One of the best available techniques for the study of coordination modes of phosphorus ylides in these compounds is ^{31}P NMR spectroscopy. P,C-coordination mode of phosphorus ylides leads to a large chemical shift for both PPh_2 and bonded PCH phosphorus groups. In contrast, in the case of P-coordination mode of phosphorus ylide, only the PPh_2 moiety shows a significant higher frequency shift. The ^{31}P NMR spectra of complexes **1**–**4** show a downfield shift for the signals due to the phosphine group compared to parent ylides Y^1 and Y^2, which implies coordination of the ylides. The ^{31}P NMR spectrum of complex **1** shows two doublet peaks at around 13.18 and 31.26 ppm, which are assigned to PPh_2 and PCH, respectively. However, these two doublet peaks appeared in the ^{31}P NMR spectrum of complex **3** at around 16.73 and 17.69 ppm with the difference in that the second-order AB pattern. Also the ^{31}P NMR spectrum of complex **2** displayed two doublet peaks at around 13.27 and 40.42 ppm, along with two satellites due to ^{195}Pt–^{31}P coupling, which are assigned to PPh_2 and PCH, respectively. The ^{31}P NMR spectrum of complex **4** shows a different pattern with two doublet peaks at around 16.46 and 19.21 ppm, along with two satellite peaks due to ^{195}Pt–^{31}P coupling, which are assigned to PPh_2 and PCH, respectively.

^{1}H NMR spectroscopy can also be used to determine the coordination mode of the ligands in complexes **1**–**4**. To do this, it is necessary to evaluate the chemical shift of the signals due to the methinic proton during coordination to metal complexes. ^{1}H NMR spectra of complexes **1** and **2** displayed a downfield shift in methinic proton signals, which suggests P,C-coordination of ylide Y^1 in the Pd/Pt–[60]fullerene complexes. In contrast, the chemical shift values of this signal for complexes **3** and **4** did not show any significant change and confirms P-coordination mode of ylide Y^2 in Pd/Pt–[60]fullerene complexes (see supporting information).

Analogously, the ^{13}C NMR spectra of complexes **1** and **2** showed a downfield shift in carbonyl signals, which suggests the ligand has coordinated to the metal centre in P,C-coordinated form. However, these signals in the ^{13}C NMR spectra of complexes **3** and **4** did not show detectable chemical shift changes compared to those observed for the parent ylide Y^2, which indicates P-

TABLE 3 Controllable factors and their levels

Factor	Description	Level 1	Level 2	Level 3	Level 4
B	Base	K_2CO_3	Cs_2CO_3	NaOAC	NaF
S	Solvent	DMF	Toluene	Methanol	THF
C	Catalyst (mol%)	0.1	0.01	0.005	0.0005

TABLE 4 L_{16} orthogonal array and experimental results for Suzuki–Miyaura reaction of chloronitrobenzene and phenylboronic acid

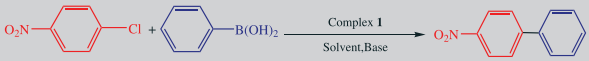

Run	Factor B	Factor S	Factor C	Yield (%)	S/N ratio
1	K_2CO_3	DMF	0.1000	98	39.8245
2	K_2CO_3	Methanol	0.0100	88	38.8897
3	K_2CO_3	Toluene	0.0050	86	38.6900
4	K_2CO_3	THF	0.0005	72	37.1466
5	Cs_2CO_3	DMF	0.0050	90	39.0849
6	Cs_2CO_3	Methanol	0.0005	82	38.2763
7	Cs_2CO_3	Toluene	0.1000	88	38.8897
8	Cs_2CO_3	THF	0.0100	84	38.4856
9	NaOAC	DMF	0.0005	84	38.4856
10	NaOAC	Methanol	0.0050	84	38.4856
11	NaOAC	Toluene	0.0100	88	38.8897
12	NaOAC	THF	0.1000	84	38.4856
13	NaF	DMF	0.0100	84	38.4856
14	NaF	Methanol	0.1000	84	38.4856
15	NaF	Toluene	0.0005	80	38.0618
16	NaF	THF	0.0050	82	38.2763

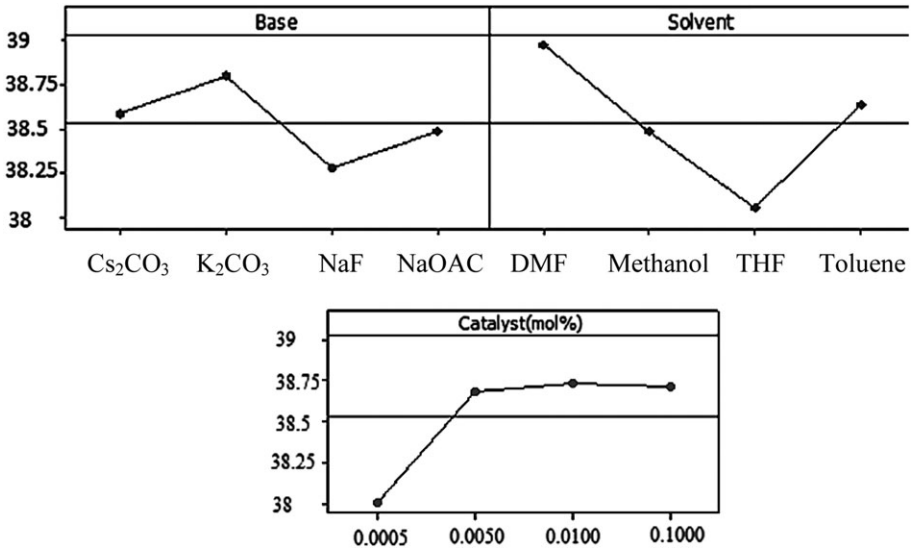

FIGURE 7 Main effect of each factor by S/N ratios

coordinated form of the ligand (see supporting information). Characterization of the [60]fullerene skeleton in ^{13}C NMR spectra of all complexes was also confirmed by observation of signals at around 141–147 ppm.

3.2.3 | UV–visible spectra

Electronic absorption spectra for solutions of the all complexes suggest the complexation of Pd and Pt through η^2-coordination on the C_{60} cage. Figure 2 shows the UV–visible spectra of complexes **1**–**4**. The most characteristic bands observed in the spectra of complexes **1**–**4** are the metal-to-ligand charge transfer bands at 316, 324 and 364 nm.

3.2.4 | Scanning electron microscopy

SEM images of pure C_{60} and complex **3** are presented in Figure 3. It can be observed from the SEM image (Figure 3a) that the C_{60} particles were irregular in shape. The size of particles was inhomogeneous, covering a range from 50 to 100 nm. The particles were so strongly aggregated that discrete particles were impossible to find and an average particle size was difficult to obtain. It can be observed from the SEM image that the surface of pure C_{60} crystals is quite smooth. However, the surface of complex **3** (Figure 3b,c) is different and the entire surface loses the smoothness.

3.3 | Cytotoxicity and Cellular Uptake Assay

The viability of normal HUVECs was evaluated after 24 h of exposure to various concentrations of compounds **2** and **4** using the MTT method as described in Section 2.3. As shown in Figure 4, neither compound was able to induce cytotoxicity in normal HUVECs, up to a concentration of 200 μM.

TABLE 5 Results of ANOVA

Source	DF[a]	Seq. SS[b]	Adj. SS[c]	Adj. MS[d]	*F*[e]	ρ (%)
B	3	62.75	62.75	20.9167	3.21374	13.83
S	3	166.75	166.75	55.5833	6.45055	36.75
C	3	140.75	140.75	46.9167	4.68132	31.02
Error	3	32.75	32.75	7.5833		
Total	15	453.75				

[a]DF: degrees of freedom.
[b]Seq. SS: sequential sum of squares.
[c]Adj. SS: adjusted sum of squares.
[d]Adj. MS: adjusted mean of squares.
[e]*F*: variance ratio.

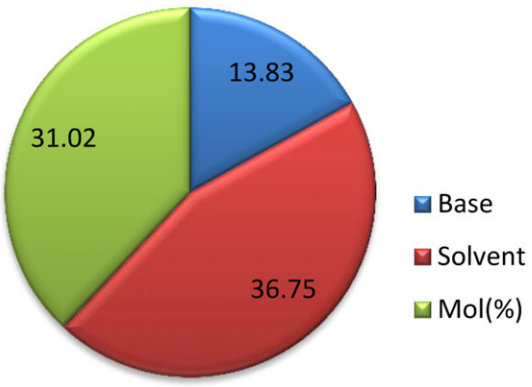

FIGURE 8 Contribution percentageρ of factors for yield of Suzuki-Miyaura coupling reaction

Pt–cyclopropa[60]fullerene complexes are used as a platform for effective drug delivery to molecular targets in tumour cells.[32] However, *in vitro* and *in vivo* detection of these nanomaterials is limited by their very low fluorescence quantum yield. The accumulation of fullerene and its derivatives in cells is particularly difficult to measure using standard fluorescence microscopy because their fluorescence is barely detectable as a result of their low solubility.[27] Use of specific Pt–cyclopropa[60]fullerene complexes for targeted delivery of drugs to tumour cells is one of the most appropriate ways for reducing the severe toxicity of conventional anticancer drugs towards normal tissues. In the current study, fluorescence microscopy images after 4 h incubation at 200 μM showed almost every cell was stained green with clear cell borders, indicating a very effective uptake of these complexes (Figure 5). Taken together, these results showed that the new Pd/Pt–cyclopropa[60]fullerene complexes can be used as non-toxic labels for cellular imaging application.

3.4 | Theoretical Study

Recently, we investigated the nature of the metal–ligand bond in some palladacyclopropa[60]fullerene complexes. Herein, we study the nature of the bonding in some similar palladium complexes using density functional theory. All geometry optimizations in this study were performed with the Gaussian 09 program.[41] Geometry optimization of (η^2-C_{60})M(Y^1), (η^2-C_{60})M(Y^2), (η^2-C_{60})M(Y^1)$_2$ and (η^2-C_{60})M(Y^2)$_2$ (M = Pd or Pt) complexes was carried out at the BP86/LANL2MB level of theory and the optimized complexes are shown in Figure 6. The Cartesian atomic coordinates of all compounds are reported in the supporting information. We note that in these complexes the Pd and Pt atoms can be coordinated to two different types of C—C bonds in the C_{60} molecule. In fact, in the C_{60} structure there are two types of bonds: the bonds at the junction of two hexagons, [6,6]-bonds, and those between one pentagon and one hexagon, [5,6]-bonds. In this study, similar to our previous work and based on experimental observations for similar complexes, we have assumed that the Pd atom is only attached to a [6,6]-double bond.

In continuation, the ADF 2013 program with energy decomposition analysis (EDA) was employed. We studied the nature of the palladium–C_{60}(fragment A), palladium–Y(fragment B), platinum–C_{60}(A) and platinum–Y(B) bonds in (η^2-C_{60})Pd(Y^1), (η^2-C_{60})Pd(Y^3), (η^2-C_{60})Pd(Y^1)$_2$, (η^2-C_{60})Pd(Y^3)$_2$, (η^2-C_{60})Pt(Y^1), (η^2-C_{60})Pt(Y^3), (η^2-C_{60})Pt(Y^1)$_2$ and (η^2-C_{60})Pt(Y^3)$_2$ complexes at the BP86-D3/TZP//BP86/LANL2DZ level of theory. In general, EDA decomposes the interaction energy between two considered fragments A and B into four terms which can be interpreted in a chemically meaningful way. The four terms are the quasi-classical electrostatic interaction between the frozen charges of the fragments (ΔE_{elec}); the exchange (Pauli) repulsion between electrons possessing the same spin (ΔE_{Pauli}); the orbital interaction term (ΔE_{orb}); and the dispersion contributions (ΔE_{disp}).

The EDA results are presented in Table 2. Our calculations indicate that in all (η^2-C_{60})MY complexes (M = Pt or Pd; Y = Y^1 or Y^3) the interaction energy values, ΔE_{int}, between (η^2-C_{60})M and Y fragment are larger than those between (η^2-C_{60}) and MY fragment. The results also show that the total interaction energies, ΔE_{int}, of both (η^2-C_{60})—MY and (η^2-C_{60})M—Y bonds in Pt complexes are larger than those in corresponding Pd complexes. As can be seen in Table 2, the values of all ΔE_{Pauli}, ΔE_{elec}, ΔE_{orb} and ΔE_{disp} terms for both (η^2-C_{60})—MY and (η^2-C_{60})M—Y bonds in Pt complexes are larger than those in corresponding Pd complexes. Indeed, the larger interaction energy in Pt complexes, in comparison with Pd complexes, is the result of the considerably larger values of ΔE_{elec} and ΔE_{orb} terms for Pt complexes. On the other hand, the percentage contributions of ΔE_{orb} and ΔE_{elec} in total interaction energy for Pt complexes do not differ considerably from those for corresponding Pd complexes. However, in both Pt and Pd complexes the percentage contribution of ΔE_{elec} in total interaction energy is considerably larger than that of

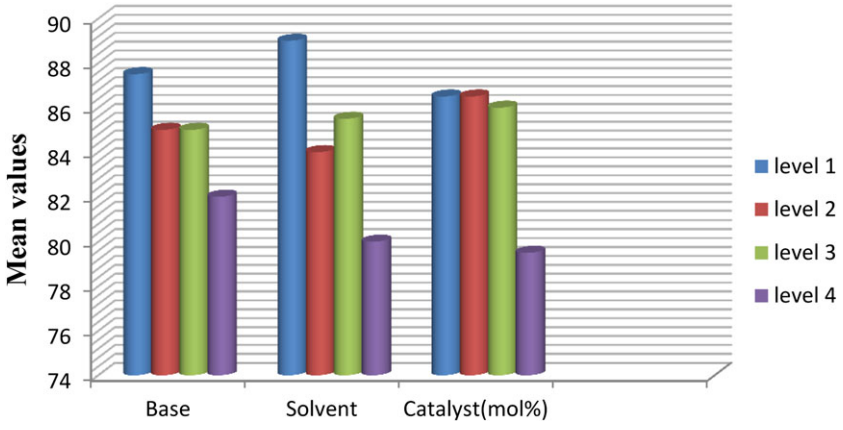

FIGURE 9 The response graph illustrating the variation of the mean yield values plotted against various extraction parameters

ΔE_{orb}. Thus, in agreement with results of our previous studies, in all complexes the $(\eta^2\text{-}C_{60})M—(Y^1)$ bond is considerably more electrostatic in nature than the $(\eta^2\text{-}C_{60})—M(Y^1)$ bond.

As we saw in Section 2, the ylides Y^1 and Y^2 form P,C- and P,P-coordinated complexes $(\eta^2\text{-}C_{60})M(Y^1)$ and $(\eta^2\text{-}C_{60})M(Y^2)_2$, respectively. In order to explain the difference between the complexes of Y^1 and Y^2 with $(\eta^2\text{-}C_{60})M$, we studied reactions (1) and (2) for Pd complexes and reactions (3) and (4) for Pt complexes:

$$(\eta^2\text{—}C_{60})Pd(Y^1) + Y^1 \rightarrow (\eta^2\text{—}C_{60})Pd(Y^1)_2 \quad (1)$$
$$\Delta E = 7.53 \text{ kcal mol}^{-1}$$

$$(\eta^2\text{—}C_{60})Pd(Y^2) + Y^2 \rightarrow (\eta^2\text{—}C_{60})Pd(Y^2)_2 \quad (2)$$
$$\Delta E = -4.25 \text{ kcal mol}^{-1}$$

$$(\eta^2\text{—}C_{60})Pt(Y^1) + Y^1 \rightarrow (\eta^2\text{—}C_{60})Pt(Y^1)_2 \quad (3)$$
$$\Delta E = 15.27 \text{ kcal mol}^{-1}$$

$$(\eta^2\text{—}C_{60})Pt(Y^2) + Y^2 \rightarrow (\eta^2\text{—}C_{60})Pt(Y^2)_2 \quad (4)$$
$$\Delta E = 3.14 \text{ kcal mol}^{-1}$$

We note that in the above reactions Y^1 and Y^2 are added to P,C-coordinated $(\eta^2\text{-}C_{60})M(Y^1)$ and $(\eta^2\text{-}C_{60})M(Y^2)$ (M = Pd or Pt) complexes and the P,P-coordinated $(\eta^2\text{-}C_{60})M(Y^1)_2$ and $(\eta^2\text{-}C_{60})M(Y^2)_2$ complexes are produced, respectively. As can be seen in the case of Y^2 the formation of P,P-coordinated $(\eta^2\text{-}C_{60})M(Y^2)_2$ is more favoured. Note that both the above reactions are entropy-disfavoured, thus only in the case of exothermic reaction (2) can we be sure that the change of Gibbs free energy of reaction has a negative value. Thus in the case of ylide Y^2 after formation of $(\eta^2\text{-}C_{60})M(Y^2)$ complex the second molecule of ylide is added to the complex and a P,P-coordinated complex, $(\eta^2\text{-}C_{60})M(Y^2)_2$, is formed. Indeed, the six-membered P,C-chelate ring in $(\eta^2\text{-}C_{60})M(Y^2)$ complex is not stable enough and the second molecule of ylide will be easily added to the complex.

3.5 | Catalytic Activity

3.5.1 | Optimization of reaction using Taguchi method

The catalytic activity of palladacyclopropa[60]fullerene complexes **1** and **3** in Suzuki–Miyaura coupling reactions of aryl chlorides with phenylboronic acid was then examined. Initially, we set up a systematic optimization of reactions using a Taguchi L16 experimental design. In this work, the orthogonal array, signal-to-noise ratio and analysis of variance were employed to study the performance characteristics on response.[42] The Taguchi method is a statistical approach to optimize the process parameters and expanded to improve the performance of total quality control.[43] The Taguchi method involves identification of appropriate control factors to obtain the optimum results of a process. Orthogonal arrays were used to conduct a set of experiments. To select an appropriate orthogonal array for conducting the experiments, the degrees of freedom were computed. Three selected

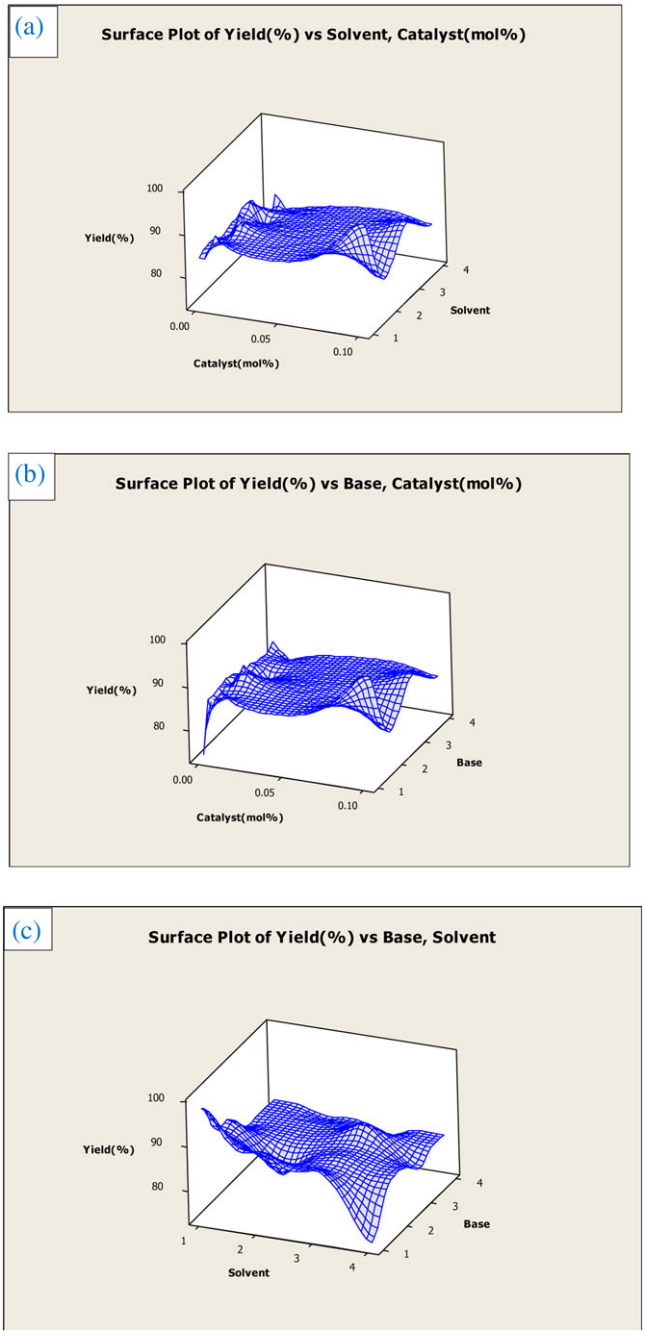

FIGURE 10 Response surface plots for the interaction between factors

factors, base (B), solvent (S) and catalyst loading (C), were used with their levels (Table 3).[44]

The most suitable orthogonal array for experimentation is an L16 array as presented in Table 4. Therefore, a total 16 experiments were carried out. In contrast, the full factorial experimental design requires $3^4 = 81$ different experiments to evaluate the influencing factors. Results of these experiments were used to analyse the data and predict the quality of components produced. Table 4 presents the required experiments to optimize the batch system which were designed using the Taguchi method. Initially, we carried out a model reaction to optimize the reaction conditions including solvent, base and catalyst loading. In each run, commonly used bases and solvents, including organic and inorganic bases and polar protic solvents and non-polar aprotic solvents, were investigated. Also, different amounts of catalyst loadings (mol%) were used at different temperatures to find optimum reaction conditions. All experiments were repeated and the yield percentage of reaction was calculated for each experiment.[45]

We applied the signal-to-noise (S/N) ratio to evaluate the experimental data. The S/N ratio analysis chosen was the-larger-the-better.[45] According to the values of mean S/N ratio shown in Table 4, the optimum level of each factor was determined from the highest value of S/N ratio and the results are exhibited in Figure 7. The optimum conditions were found to be base: K_2CO_3, Cs_2CO_3; solvent: DMF, toluene; catalyst loading: 0.005, 0.01 and 0.1 mol%.

Analysis of variance (ANOVA) was used to evaluate the response magnitude (%) of each parameter in the orthogonal experiment. To determine the optimum conditions for yield of experiments, we used the relationship between each parameter and the percentage contribution ρ and ANOVA.[46–48] *F*-statistics illustrates the significance of each factor on the response quality.

Table 5 presents the ANOVA results obtained from experimental data. The solvent with the highest *F*-value of 6.45 has the highest percentage contribution (36.75%) to the yield. Moreover, catalyst loading and base play important roles in the yield with *F*-value and percentage contribution. Based on Table 5, solvent has the largest pure sum of squares and largest percentage contribution to the yield of Suzuki–Miyaura coupling reaction. Therefore, it was concluded that solvent is the most important factor affecting the yield. The percentage contribution of each factor is shown in Figure 8. Also, the variation of the mean yield values against various extraction parameters is shown in Figure 9.

The surface plots shown in Figure 10 should be of help in better finding out the interaction effects of the experimental factors on the yield percentage. The interaction effect of solvent and catalyst loading, as shown in Figure 10(a), indicates that polar solvents such as DMF were more efficient for the yield of compounds up to 98%, while a polar aprotic solvent gave a comparatively good yield and the lowest yield (72%) was obtained with tetrahydrofuran (THF) as solvent. This could be due to the reflux temperature of the solvent, and with an increase in catalyst loading, the yield percentage increased. Also, the interaction surface plot of the base and catalyst loading is shown in Figure 10(b). The effect

TABLE 6 Suzuki–Miyaura coupling reaction of functionalized aryl chlorides[a]

Entry	R	Catalyst	Product	Yield (%)[b]
1	NO_2	**1**	4-Nitrobiphenyl (**5a**)	93
2	NO_2	**3**		90
3	CHO	**1**	4-Phenylbenzaldehyde (**5b**)	97
4	CHO	**3**		92
5	H	**1**	Biphenyl (**5c**)	85
6	H	**3**		80
7	COOH	**1**	4-Phenylcarboxylic acid (**5d**)	95
8	COOH	**3**		92
9	$COCH_3$	**1**	4-Acetylbiphenyl (**5e**)	90
10	$COCH_3$	**3**		86

[a]Reaction conditions for Suzuki–Miyaura coupling reaction: aryl chloride (0.5 mmol), phenylboronic acid (0.75 mmol), K_2CO_3 (1 mmol), DMF (2 ml), catalyst (0.005 mol%), 130 °C, 2 h, in air.

[b]Isolated yield.

of various mineral bases on this reaction was investigated and results showed that inorganic bases were much better than organic ones, where K_2CO_3 was the best choice of base and the yield of product could be increased to 98%. The interaction effect of base and solvent is considered in Figure 10(c). Therefore, the optimal conditions for Suzuki–Miyaura coupling reaction of aryl chlorides and phenylboronic acid catalysed by complexes **1** and **3** are as follows: base: K_2CO_3; solvent: DMF; catalyst loading: 0.005 mol%.

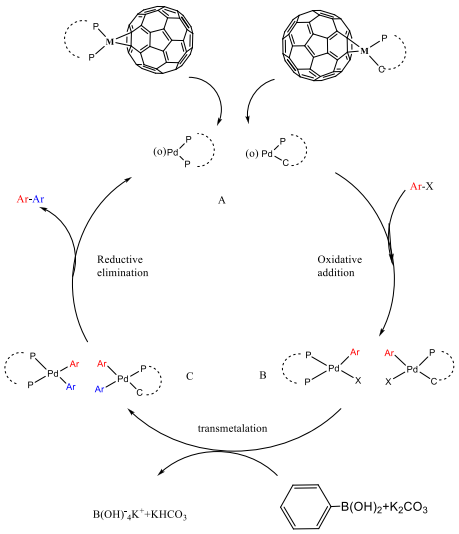

SCHEME 3 Proposed mechanism for Suzuki–Miyaura reaction catalysed by **1** and **3**

3.5.2 | Suzuki–Miyaura coupling reaction of functionalized aryl chlorides

In order to compare the catalytic activity of complexes of **1** and **3**, they were applied using the same reaction conditions. Functionalized aryl chlorides bearing electron-withdrawing groups reacted with phenylboronic acid, and corresponding coupled products were obtained in high to excellent yields (Table 6). As expected, reaction of 4-chlorobenzaldehyde with phenylboronic acid gave the desired product in highest yield. Also, the lowest conversions were observed in reaction of phenylboronic acid and 4-chlorobenzene as a neutral aryl chloride which does have not strong electron-withdrawing groups. Each of the pair of complexes **1** and **3** exhibited good catalytic activity, attributed to the Pd(0) core of their molecular structures, but the catalytic activity of **1** was higher than that of **3**. The fact that Pd(0) species in P,C-coordinated complex **1** is more efficient than that in P-coordinated complex **3** may be due to difference in coordination modes of their phosphorus ylide ligands.

An implicit mechanism of the Suzuki–Miyaura coupling reaction is proposed by comparison with literature reports to illustrate the role of ligand in various observed efficiencies (Scheme 3).[49–51] Initially, the complexes lose C_{60} in solution necessary to generate coordinatively unsaturated L_nPd^0 catalyst (**A**). This step is followed by oxidative addition of the aryl chloride, which is often the rate-determining step in C—C coupling catalytic cycles (**B**).[52,53] The phosphine is a σ-donor/π-acceptor

TABLE 7 Comparison of Suzuki–Miyaura coupling reaction of chlorobenzene and phenylboronic acid using complexes **1** and **3** with that using other catalytic systems

Entry	Pd source	Catalyst loading (mol%)	Condition	Yield (%)	Ref.
1	Binuclear palladated triphenylphosphine derivative	0.5	K_2CO_3, DMF/H_2O, 100 °C, 1 h	85	[58]
2	Pd(II) complex of nitrogen-containing bis(phosphinite)	0.1	K_3PO_4, DMF, 25 °C, 24 h	90	[59]
3	Pd(II) complex of sulfonated diimine	3	K_2CO_3, DMA, 95 °C, 1.5 h	97	[60]
4	P,C-coordinated Pd–cyclopropa[60]fullerene complex	0.005	K_2CO_3, DMF, 130 °C, 2 h	93	This work
5	P-coordinated Pd–cyclopropa[60]fullerene complex	0.005	K_2CO_3, DMF, 130 °C, 2 h	90	This work

ligand and it can decrease electron density on the metal with an additional π-interaction (π-backbonding).[54] The carbene has strong σ-donor and relatively weak π-acceptor interactions and it can increase the electron density on the metal centre,[55] which destabilizes the carbon–halogen bond, leading to faster cleavage and eventually oxidative addition to Pd. The catalytic cycle is continued by a transmetallation step, in which an aryl group transfers to Pd centre from the organoboron compound, activated by K_2CO_3 base (**C**).[56] Finally, reductive elimination of intermediate **C** produces the desired coupling product and regenerates the L_nPd^0 active catalyst which starts another catalytic cycle.[57]

A comparison between the catalytic activities of the present complexes and other Pd catalysts having different ancillary ligands in Suzuki–Miyaura reaction was carried out. The results indicated that the differences in catalytic behaviour presented in Table 7 should be ascribed not only to the differences in the experimental conditions (e.g. effects of solvent, base, temperature and catalyst loading), but also mainly attributed to the characteristic differences in the Pd content. The donor atoms of ligands have a substantial effect on stabilization and consequently on the performance of Pd catalyst and the ligand-controlling conditions are clearly obvious in such catalytic reactions carried out under similar experimental conditions.

4 | CONCLUSIONS

The present study describes the synthesis and characterization of new Pd/Pt–cyclopropa[60]fullerene complexes containing unsymmetric phosphorus ylides. According to the results of NMR (^{1}H, ^{13}C and ^{31}P), IR, UV–visible and SEM analyses, the structures of products were successfully characterized experimentally and theoretically. The results indicate that the phosphorus ylide Y^1 coordinates to Pd and Pt in P,C-coordinated form, while phosphorus ylide Y^2 coordinates to these metal centres through free phosphorus atom as P-coordinated form. Also, the results of cytotoxicity and cellular uptake assay of Pt complexes **2** and **4** showed that nanoparticles of these complexes can be used as non-toxic labels for cellular imaging application. Furthermore, Pd complexes **1** and **3** were applied as efficient catalysts in Taguchi-optimized Suzuki–Miyaura coupling reactions of various aryl chlorides and phenylboronic acid, resulting in good to excellent yields of coupled products. The results also indicated that the Taguchi method is a suitable approach for optimization of parameters in Suzuki–Miyaura coupling reactions.

ACKNOWLEDGEMENT

Funding of our research from Bu-Ali Sina University is gratefully acknowledged.

ORCID

Seyyed Javad Sabounchei http://orcid.org/0000-0001-9000-5304
Sadegh Salehzadeh http://orcid.org/0000-0003-2840-1896
Farahnaz Maleki http://orcid.org/0000-0002-5747-1319
Leila Hosseinzadeh http://orcid.org/0000-0003-0536-3209

REFERENCES

[1] H. W. Kroto, J. R. Heath, S. C. Brien, R. F. Curl, R. E. Smalley, *Nature* **1985**, *318*, 162.

[2] A. V. Eletskii, *Physics-Uspekhi* **2000**, *43*, 170.

[3] R. J. Patterson, A. S. Catledge, Y. K. Vohra, *Phys. Rev. Lett.* **2000**, *85*, 5364.

[4] A. Goel, P. Hebgen, J. B. V. Sande, J. B. Howard, *Carbon* **2002**, *40*, 177.

[5] J. Bernholc, D. Brenner, M. B. Nardelli, V. Meunier, C. Roland, *Annu. Rev. Mat. Res.* **2002**, *32*, 347.

[6] S. Bronnikov, A. Podshivalov, S. Kostromin, M. Asandulesa, V. Cozan, *Phys. Lett. A* **2017**, *381*, 796.

[7] S. Filippone, N. Martin, in *Encyclopedia of Polymeric Nanomaterials*, (Eds: S. Kobayashi, K. Müllen), Springer, Berlin **2015** 755.

[8] A. A. Popov, S. Yang, L. Dunsch, *Chem. Rev.* **2013**, *113*, 5989.

[9] D. Soto, R. Salcedo, *Molecules* **2012**, *17*, 7151.

[10] T. M. Figueira-Duarte, A. Gegouta, J. F. Nierengarten, *Chem. Commun.* **2007**, 109.

[11] J. M. Campanera, J. Munoz, J. Vazquez, C. Bo, J. M. Poblet, *Inorg. Chem.* **2004**, *43*, 6815.

[12] B. C. Thompson, J. M. J. Fréchet, *Angew. Chem. Int. Ed.* **2008**, *47*, 58.

[13] L.-C. Song, G.-A. Yu, F.-H. Su, Q.-M. Hu, *Organometallics* **2004**, *23*, 4192–4198.

[14] L.-C. Song, G.-A. Yu, H.-T. Wang, F.-H. Su, Q.-M. Hu, Y.-L. Song, Y.-C. Gao, *Eur. J. Inorg. Chem.* **2004**, 866.

[15] L.-C. Song, G.-A. Yu, Q.-M. Hu, C.-M. Che, N. Zhu, J.-S. Huang, *J. Org. Chem.* **2006**, *691*, 787.

[16] J. S. Fletcher, N. P. Lockyer, J. C. Vickerman, *Surf. Interface Anal.* **2006**, *38*, 1393.

[17] R. Bakry, R. M. Vallant, M. Najam-ul-Haq, M. Rainer, Z. Szabo, C. W. Huck, G. K. Bonn, *Int. J. Nanomedicine* **2007**, *2*, 639.

[18] S. J. Sabounchei, M. Ahmadi, Z. Nasri, E. Shams, S. Salehzadeh, Y. Gholiee, R. Karamian, M. Asadbegy, S. Samiee, *C. R. Chim.* **2013**, *16*, 159.

[19] S. J. Sabounchei, M. Hosseinzadeh, M. Panahimehr, D. Nematollahi, H. R. Khavasi, S. Khazalpour, *Transition Met. Chem.* **2015**, *40*, 657.

[20] S. J. Sabounchei, H. Nemattalab, S. Salehzadeh, S. Khani, M. Bayat, H. R. Khavasi, *Polyhedron* **2008**, *27*, 2015.

[21] S. J. Sabounchei, S. Samiee, M. Pourshahbaz, S. Salehzadeh, M. Bayat, D. Nematollahi, R. Karamian, M. Asadbegy, *J. Chem. Res.* **2014**, *38*, 35.

[22] S. J. Sabounchei, M. Zamanian, M. Pourshahbaz, M. Bayat, R. Karamian, M. Asadbegy, *J. Chem. Res.* **2016**, *40*, 130.

[23] S. J. Sabounchei, M. Sarlakif, S. Salehzadeh, M. Bayat, M. Pourshahbaz, H. R. Khavasi, *Polyhedron* **2012**, *38*, 131.

[24] E. P. Urriolabeitia, *Dalton Trans.* **2008**, *42*, 5673.

[25] J. Vicente, M. T. Chicote, J. Fernandez-Baeza, F. J. Lahoz, J. A. Lopez, *Inorg. Chem.* **1991**, *30*, 3617.

[26] N. F. Goldshleger, *Fullerene Sci. Technol.* **2001**, *9*, 255.

[27] H. Veisi, R. Masti, D. Kordestani, M. Safaei, O. Sahin, J. Mol, *Catal. A* **2014**, *385*, 61.

[28] A. Fihri, M. Bouhrara, B. Nekoueishahraki, J. M. Basset, V. Polshettiwar, *Chem. Soc. Rev.* **2011**, *40*, 5181.

[29] F. Giacalone, V. Campisciano, C. Calabrese, V. La Parola, Z. Syrgiannis, M. Prato, M. Gruttadauria, *ACS Nano* **2016**, *10*, 4627.

[30] Z. Zhang, T. Sun, C. Chen, F. Xiao, Z. Gong, S. Wang, *ACS Appl. Mater. Interfaces* **2014**, *6*, 21035.

[31] R. R. Panchuk, S. V. Prylutska, V. V. Chumak, N. R. Skorokhyd, L. V. Lehka, M. P. Evstigneev, I. Prylutskyy Yu, W. Berger, P. Heffeter, P. Scharff, U. Ritter, R. S. Stoika, *J. Biomed. Nanotechnol.* **2015**, *11*, 1139.

[32] A. Andreoni, L. Nardo, M. Bondani, B. Zhao, J. E. Roberts, *J. Phys. Chem.* **2013**, *117*, 7203.

[33] S. K. Sharma, L. Y. Chiang, M. R. Hamblin, *Nanomedicine* **2011**, *6*, 1813.

[34] I. Yanov, J. Leszczynski, E. Sulman, V. Matveeva, N. Semagina, *Quantum Chem.* **2004**, *100*, 810.

[35] J. T. Tsai, T. K. Liu, J. H. Chou, *IEEE Trans. Evol. Comput.* **2004**, *8*, 365.

[36] S. J. Sabounchei, S. Samiee, S. Salehzadeh, Z. Bolboli Nojinib, I. Erranc, *J. Org. Chem.* **2010**, *695*, 1441.

[37] Y. C. Lin, H. H. Hsueh, S. Kanne, L. K. Chang, F. C. Liu, I. J. B. Lin, G. H. Lee, S. M. Peng, *Organometallics* **2013**, *32*, 3859.

[38] M. R. Smith, Y. J. Jang, J. Y. Kim, M. A. Ciufolini, *Tetrahedron* **2013**, *69*, 10139.

[39] L. Nagashima, H. Nakaoka, A. Tajima, S. Saito, Y. Itoh, *Chem. Lett.* **1992**, *21*, 1361.

[40] M. Kalyanasundari, K. Panchanatheswaran, W. T. Robinson, H. Wen, *J. Org. Chem.* **1995**, *491*, 103.

[41] M. J. Frisch, *Gaussian 09, Revision A.02*, Gaussian Inc., Wallingford, CT, **2009**.

[42] S. Athreya, Y. D. Venkatesh, *Int. Ref. J. Eng. Sci. (IRJES)* **2012**, *1*, 13.

[43] A. Schoonen, M. T. Schoonen, *J. Colloid Interface Sci.* **2014**, *422*, 1.

[44] E. O. Doebelin, D. N. Manik, *Measurement Systems: Application and Design*, Tata McGraw-Hill, New Delhi **2007**.

[45] J. Zolgharnein, N. Asanjarani, T. Shariatmanesh, *Int. Biodeter. Biodegr.* **2013**, *85*, 66.

[46] B. Ramavandi, G. Asgari, J. Faradma, S. Sahebi, B. Roshani, *Korean J. Chem. Eng.* **2014**, *31*, 2207.

[47] C. S. Chou, R. Y. Yang, J. H. Chen, S. W. Chou, *Powder Technol.* **2010**, *199*, 264.

[48] N. J. Cox, J. Warburton, A. Armstrong, V. J. Holliday, *Earth Surf. Process. Landf.* **2008**, *33*, 25.

[49] A. Suzuki, *J. Org. Chem.* **1999**, *576*, 147.

[50] S. Kozuch, J. M. L. Martin, *ACS Catal.* **2011**, *1*, 246.

[51] C. Len, S. Bruniaux, F. Delbecq, V. S. Parmar, *Catalysts* **2017**, *7*, 146.

[52] R. Martin, S. L. Buchwald, *Acc. Chem. Res.* **2008**, *41*, 1461.

[53] M. G. Speziali, A. G. Marques da Silva, D. M. Vaz de Miranda, A. L. Monteiro, P. A. Robles-Dutenhefner, *Appl. Catal. A* **2013**, *462*, 39.

[54] M. P. Mitoraj, A. Michalak, *Inorg. Chem.* **2010**, *49*, 578.

[55] N. S. Antonova, J. J. Carbo, J. M. Poblet, *Organometallics* **2009**, *28*, 4283.

[56] J. M. Neely, M. J. Bezdek, P. J. Chirik, *ACS Cent. Sci* **2016**, *2*, 935.

[57] R. Jana, T. P. Pathak, M. S. Sigman, *Chem. Rev.* **2011**, *111*, 1417.

[58] S. Yasar, C. Sahin, M. Arslan, I. Ozdemir, *J. Org. Chem.* **2015**, *776*, 107.

[59] N. Shahnaz, B. Banik, P. Das, *Tetrahedron Lett.* **2013**, *54*, 2886.

[60] M. Thimmaiah, S. Fang, *Tetrahedron* **2007**, *63*, 6879.

SUPPORTING INFORMATION

Additional Supporting Information may be found online in the supporting information section at the end of the article.

How to cite this article: Sabounchei SJ, Badpa K, Hashemi A, Salehzadeh S, Maleki F, Hosseinzadeh L. Synthesis, characterization and theoretical and fluorescence emission microscopy studies of new Pd/Pt–cyclopropa[60]fullerene complexes: Application of Taguchi method for optimization of parameters in Suzuki–Miyaura reaction. *Appl Organometal Chem*. 2018;e4382. https://doi.org/10.1002/aoc.4382